Research Square

Preprints are preliminary reports that have not undergone peer review.
They should not be considered conclusive, used to inform clinical practice,
or referenced by the media as validated information.

Highly efficient ion sieving through angstrom-scale channels embedded with supramolecular coordination complexes

Yue Sun (sunyue@tiangong.edu.cn)
Tiangong University
Runhao Li
South-Central University for Nationlities
Shi-Qi Cheng
South-Central University for Nationlities
Zhao Chen
Jiangxi Science and Technology Normal University
Yao Xu
Chinese University of Hong Kong
Fan Yi
South-Central University for Nationlities
Huan Qin
South-Central University for Nationalities
Xiao-Cui Liang
South-Central University for Nationalities
Yi Liu
Wuhan University of Science and Technology

Article

Keywords:

Posted Date: April 26th, 2022

DOI: https://doi.org/10.21203/rs.3.rs-1514301/v1

License: This work is licensed under a Creative Commons Attribution 4.0 International License.
Read Full License

Abstract

Artificial channels that mimic biological systems are of significant interest but their fabrication remains challenging. The well-defined platinum(II) based supramolecular coordination complexes **1** was prepared *via* the directional bonding of supramolecular coordination complexes. These were attached to the inner walls of a solid polyethylene terephthalate channel having a bullet-like morphology based on self-assembled interfacial growth. The resulting channels allowed the rapid transport of monovalent metal ions (K^+, Na^+ and Li^+) from tip to base while inhibiting the migration of divalent ions (Mg^{2+} and Ca^{2+}). These channels efficiently separated monovalent from divalent metal ions on this basis, with an ultrahigh K^+/Mg^{2+} selectivity ratio of 1015.5. Theoretical simulations demonstrated that this selectivity resulted from the high dehydration energy of the divalent ions and their strong interactions with porphyrin groups on the supramolecular coordination complexes. The present work is expected to assist in the future design of functionalized ion channels as well as the development of separation membrane materials.

Introduction

Biological transmembrane ion channels have attracted considerable attention because of their potential applications in many fields, such as sensing, separation, and catalysis.[1–7] A well-known example is the Na^+ channel, which has a complex protein-based architecture with a central cavity approximately 12 Å in size.[8,9] This channel is able to selectively filter ions based on a size limit of 3 to 5 Å and thus preferentially selects for Na^+ over other ions such as K^+ or Ca^{2+}. Inspire by such naturally occurring protein channels, solid state channels have received widespread attention in recent years, especially because these channels may have applications in ions separation because of their stable mechanical properties, potential for functionalization and tunable shapes and sizes.[10–22] Artificial solid state channels are usually designed by functionalizing the inner surfaces of channels with specific molecules.[23–38] The resulting channels can exhibit gating responses such as opening and closing in reaction to external stimuli. However, the gating effects of these channels are typically very weak because they tend to be relatively large compared with ions and thus are not able to completely block ion transport even in the closed state. Hence, the design of selectively permeable, angstrom-sized channels would allow greater mimicry of biological membranes and could lead to applications such as ion sieving and water filtration.

Supramolecular coordination complexes (SCCs) that permit precise adjustment of shape and geometry have been used for the construction of functional molecular architectures.[39–43] Notably, Tecilla *et al*. demonstrated that a tetraporphyrin metallacycle can empower the formation of nanopores in a liposomial membrane.[43] A better understanding of the confined mass-transport properties in such channels could permit the rational design of structures with high efficiency. However, the concentrations of the various precursors in such structures are affected by the partitioning of these compounds between bulk water and complicated mem-brane environments, which may lead to complex mixtures of species with variations in stoichiometry. The possibility that angstrom-sized solid channels could be fabricated

using well-defined SCCs is particularly attractive. Thus, there is an urgent need to develop stable SCCs-based channel systems related to the study of ion channels.

Herein, inspired by biological ion channels, the SCCs **1** having a well-defined size and shape could be synthesized based on the principle of directional bonding by combining the pyridine-functionalized porphyrin organic ligand **2** and the 180° platinum(II) metal ligand **3**. We readily fabricated an asymmetrically structured solid state channel with angstrom-scale pore sizes and having rectifying characteristics *via* immobilizing a platinum(II) based SCCs **1** into a solid polyethylene terephthalate channel (Fig. 1). This channel also exhibited the ability to filter metal cations. Remarkably, dual ion permeation experiments confirmed that this hybrid channel was capable of the efficient separation of K^+/Mg^{2+}, Na^+/Mg^{2+} and Li^+/Mg^{2+} ions with selectivity ratios of 1015.5, 485.3 and 288.2, respectively. Molecular dynamics (MD) simulations and density functional theory (DFT) calculations were used to study the mechanisms at work in the confined channel. These analyses demonstrated that the narrow cavity of the SCCs and interactions between the various ions and the porphyrin moieties both contributed to the high mono/divalent ion mobility ratios in the hybrid channel. These effects resulted in ultrahigh K^+/Mg^{2+} selectivity because of their significant differences in dehydration energy and binding affinity within SCCs channel, while the dehydration required for the selective permeation of ions in atomic-scale sieves. Potential of mean force (PMF) profiles for the movement of metal ions through the channel indicated that the energy barrier to the migration of Mg^{2+} ions through a single window of the SCCs channel was approximately 6.5 times higher than that of K^+. The present work demonstrates an approach to developing SCCs-based channels for ion separation, power generation and energy storage.

Results

Fabrication of SCCs-based hybrid channel

The SCCs **1** was readily synthesized from precursor **2** and precursor **3** (Fig. 1d). Multinuclear and ^1H-^1H correlated spectroscopy nuclear magnetic resonance (NMR) spectroscopy was subsequently used to analyze the structure of the resulting material (Figures S1-S5). Protons H_a and H_b on the coordinated pyridine exhibited obvious downfield shifts relative to those of the free precursor **2**, suggesting the formation of nitrogen-platinum bonds. The $^{31}P\{^1H\}$ NMR spectrum of the SCCs **1** exhibited a singlet peak at 15.94 ppm with concomitant ^{195}Pt satellites and was obviously shifted upfield compared with the peak generated by the precursor **3**. These results demonstrated the formation of a highly symmetric network-type SCCs with a single phosphorus environment (Fig. 1e and 1f). Small angle X-ray scattering (SAXS) data and pore size distribution profiles obtained from N_2 adsorption isotherms showed that the pore sizes in this material were in the range of 0.9-4 nm (Figures S6 and S7). The Materials Studio software package was used to simulate the two different stacking modes of the SCCs: AA type (providing a pore size of 4 nm) and AB type (with a pore size of 0.9 nm), as shown in Fig. 1g and 1h. The simulation was in good agreement with the experimental data and suggested that the AB stacking mode was preferred. The SCCs-based channel was fabricated by the interfacial self-assembly of SCCs to form a single bullet-like

morphology (Fig. 1b and 1c). In this process, a polyethylene terephthalate (PET) membrane was etched using an ion track apparatus together with a surfactant modifier to expose terminal benzoic acid groups on membrane walls. These groups served as ligands and assisted in the self-assembly of the SCCs in the confined channel based on the coordination of platinum(II) atoms with the deprotonated carboxyl groups. Scanning electron microscopy (SEM) images of cross-sections of the PET membrane clearly showed the formation of a bullet-like channel with tip and base diameters of 60.8 ± 17.1 nm and 346.3 ± 67.5 nm, respectively. These results confirmed the successful formation of a channel, and a comparison of images acquired before and after modification of the PET with the SCCs demonstrated the assembly of the complex (Figs. 2a and 2b). Energy dispersive X-ray spectroscopy (EDS) mapping showed Pt, P and S signals across the entire hybrid channel (Fig. 2c) while X-ray photoelectron spectroscopy (XPS) of the membrane demonstrated the appearance of a Pt signal (Fig. 2d). In addition, fourier transform infrared (FT-IR) spectroscopy exhibited the presence of the –C ≡ C– stretch at 2125 cm^{-1} in contrast to that of the bare membrane (Fig. 2e). The contact angle of the membrane after modification with the SCCs was increased from 62.7 ± 1.2° to 77.2 ± 1.4° (Fig. 1f). X-ray diffraction (XRD) patterns acquired from the channel before and after attaching the SCCs provided further evidence for the formation of a hybrid channel (Figure S9).

Metal ion transport in a hybrid channel

Ion transport within a single bullet-like channel before and after modification with SCCs was assessed by measuring transmembrane ion currents. During these trials, current-voltage (*I-V*) data were collected in electrolyte solutions containing KNO_3, $NaNO_3$, $LiNO_3$, $Ca(NO_3)_2$ or $Mg(NO_3)_2$ at a concentration of 0.1 M. The bare channel generated an asymmetric *I-V* curve in each of these electrolyte solutions, and these data suggested rectification based on the rapid preferential migration of positively charged metal ions from the channel tip to base (Fig. 3a). This rectification effect was primarily attributed to the formation of a metal ion concentration gradient along the asymmetric bare channel resulting from the deprotonated carboxyl groups on the interior surfaces. These factors promoted the transport of cations from the tip to base and inhibited movement of these ions in the opposite direction. Figure 3a indicates that the ion current in the bare channel ranged from − 34 to -80 nA at -2 V as the various cation salts moved in the preferred direction, resulting in some partitioning of the metal ions. We defined the ratio of the ion current from the tip to base to that from the base to tip ($|I_{-2V}|/|I_{+2V}|$) as the ion rectification ratio. The rectification ratios for the monovalent nitrates ($LiNO_3$, $NaNO_3$, KNO_3) were 16.6, 18.0 and 18.5, respectively, while the values for the divalent nitrates ($Mg(NO_3)_2$ and $Ca(NO_3)_2$) were 8.0 and 8.7, respectively. These data suggested that the bare channel would be able to serve as a suitable platform for the immobilization of SCCs. Interestingly, the *I-V* curves of the functionalized channels after modification with SCCs showed much higher rectification ratios in trials with the monovalent nitrates after modification (14.2 for $LiNO_3$, 20.9 for $NaNO_3$, 25.5 for KNO_3) compared with those of the bare channel (Fig. 3b). We suggest that this result can be ascribed to the presence of the highly positively charged SCCs having angstrom-sized pores in the tip region. These complexes would be expected to modify the charge distribution and pore size to produce much greater asymmetry.

The conductance (G) values of the channels were also assessed. No significant differences were observed during trials with the monovalent nitrates before and after modification with the SCCs at -2 V (Fig. 3c). However, the conductance values observed with the divalent nitrates were sharply decreased in the case of the SCCs channel at -2 V, such that these values were much lower than those obtained using the monovalent nitrates. Upon applying the same voltage to the SCCs channel, the differences in ion conductance greatly contributed to the metal ion conduction variations in the salt solutions containing the identical anion (NO_3^-). The selectivity ratios for the K^+/Mg^{2+}, Na^+/Mg^{2+}, Li^+/Mg^{2+} and Ca^{2+}/Mg^{2+} ion pairs in the bare channel at -2 V were 4.7, 3.5, 2.4 and 1.1, respectively, as calculated using equation S1. In contrast, following modification with the SCCs, the corresponding selectivity ratios were increased to 1223.2, 801.4, 543.4 and 3.3, respectively (Fig. 3d). The effect of the electrolyte concentration was examined by varying the concentration from 0.05 to 1.0 M (Figure S10) and the K^+ and Mg^{2+} conductance of the SCCs-based channel was found to increase along with the electrolyte concentration (Fig. 4a). The K^+/Mg^{2+} selectivity ratio of the hybrid channel at -2 V also increased from 1167.8 to 1223.2 as the concentration was increased from 0.05 to 0.1 M and then decreased to 699.7 as the concentration was further increased to 1.0 M (Fig. 4b). The Na^+/Mg^{2+} selectivity ratio exhibited the same general trend, while the Li^+/Mg^{2+} selectivity ratios were smaller than the K^+/Mg^{2+} values at the same concentrations.

The ion sieving properties of the hybrid channel were also examined at different pH values (Figure S11). When immersed in water at a neutral pH, the SCCs were positively charged and were found to have a zeta potential of 23.3 ± 1.37 mV in addition to an isoelectric point of approximately 9.9 (Fig. 4c). The zeta potential increased with decreases in the pH value below the isoelectric point. In the SCCs-based channel, the KNO_3 conductance increased from 18.75 to 36.76 nS while the $Mg(NO_3)_2$ conductance decreased from 0.076 to 0.056 nS as the pH was increased from 5 to 9 (Fig. 4d). Correspondingly, the K^+/Mg^{2+} selectivity ratio increased from 492.17 to 1316.72 over the same pH range (Fig. 4e). These results indicate that the selectivity of the SCCs-based channel for the K^+/Mg^{2+} ions could be tuned by varying the pH. Dual ion separation experiments were performed at a pH of 9 and with electrolyte concentrations of 0.1 M and Fig. 3f demonstrates that the K^+/Mg^{2+} selectivity ratio was as high as 1015.5 and therefore were quite high when compared with the ion separation results previously reported based on work with artificial channels or membranes (Table S1).

Mechanism of metal ion separation in the SCCs-based hybrid channel

The cations used in this work were able to bind water molecules to form hydrated ions in aqueous solutions and all had similar hydrated ion diameters and mobilities (Table S2). Separating the metal ions using only the bare channel was difficult because the pore diameter in the channel was much larger than the hydrated diameters. However, the SCCs-based channel had a narrow diameter of approximately 8 Å that was similar to the hydrated ion diameters, meaning that the metal ions would likely need to be partially dehydrated before passing through the channel. We therefore propose that the different energies

of dehydration and binding affinities of the various cations were responsible for observed variations in mobility. The energies of hydration of divalent metal ions are much higher than those of monovalent metal ions, and therefore it follows that the former will be relatively difficult to dehydrate. Furthermore, DFT calculations performed in the present work confirmed obvious differences in the interactions between the various metal ions and the porphyrin groups of the SCCs, which would be expected to affect ion mobility (Table S3).

The ion selectivity mechanism was confirmed by simulating the metal ions transport behavior in the SCCs-based channel using MD (Figure S12). In these simulations, the SCCs was assumed to be flexible such that the organic ligands were able to rotate as ions moved through the channel. The simulated ion mobilities were found to decrease in the order of $K^+ > Na^+ > Li^+ > Ca^{2+} > Mg^{2+}$, which was consistent with the experimental conductance data. The predicted K^+/Mg^{2+} mobility ratio was determined to be 714.6 (Fig. 5a). The tensile forces associated with the passage of the metal ions through the channel were also assessed (Figure S15), and the maximum tensile force required for Mg^{2+} ions to move through the passage (approximately 92.1 kJ mol^{-1} $Å^{-1}$) was approximately six times higher than that for K^+ (approximately 15.1 kJ mol^{-1} $Å^{-1}$). This result indicated that Mg^{2+} ions would migrate through the channel much more slowly, in agreement with the calculated ion mobilities. DFT simulations were also used to study the interactions of the SCCs porphyrin groups with the metal ions and the calculated binding affinities for the divalent ions were stronger than those for the monovalent ions. These theoretical simulations demonstrated that differences in binding affinity as well as in energies of dehydration together resulted in the efficient ion selectivity of the SCCs-based channel. Additional insights into the ion separation mechanism were obtained by calculating the PMF profiles associated with the migrations of the metal ions along the SCCs-based channel (Fig. 5b). The energy barrier for the movement of a Mg^{2+} ion through one window of the channel (approximately 213.5 kJ mol^{-1}) was determined to be approximately 6.5 times higher than that of a K^+ ion (approximately 32.8 kJ mol^{-1}). Microscopic molecular snapshots based on the PMF data were generated to study the ion transport process, and these indicated that the ions could move either through the centre or the edge of each window of the SCCs channel. Specifically, the metal ions were transported through the narrow center of the channel formed by the triethyl phosphorous groups and the interlayer slits of the SCCs. Owing to the lower energy of hydration and binding affinity of the K^+ ions with porphyrins, these ions readily moved through the channel (Figs. 5c and 5d). In contrast, the Mg^{2+} ions had a higher energy of hydration and larger hydration diameter and thus almost impossible to pass through the centre of the channel. These ions were trapped by the porphyrin groups when they migrated through the interlayer slits based on the strong binding of Mg^{2+} with the porphyrin groups. As a result, the energy barrier for Mg^{2+} migration through the SCCs-based channel was much higher than that for K^+ migration.

Discussion

In summary, a well-defined SCCs **1** was synthesized from the pyridine-functionalized porphyrin organic ligand **2** and the platinum(II) metal ligand **3** according to the principle of directional bonding. These

complexes were affixed to a bare PET channel *via* interfacial growth in conjunction with self-assembly to permit ion sieving. Experimental and theoretical simulation results confirmed that the energies of hydration and the sizes of the hydrated ions as well as the interactions between porphyrins and the divalent metal ions were the key factors related to the separation of monovalent and divalent metal ions in the angstrom-scale SCCs channel. We anticipate that other types of hybrid channels with various separation behaviours, including ion sieving, could be realized in future by integrating SCCs with various membranes. Given the stability and designability of SCCs systems, this work paves the way for the development of artificial channels with applications in the field of ion separation.

Methods

Preparation of the bullet-shaped channel

A channel was produced in a PET membrane using an ion track etching technique at 65°C, with the bullet-like tip protected by adding a surfactant. In this process, one chamber was filled with the etching solution (6 M NaOH) while the other chamber was filled with a mixture of the etching solution and the surfactant (6 M NaOH in 0.025% sodium dodecyl diphenyloxide disulfonate). The etching progression was monitored by supplying a constant potential of 1 V across the membrane using a picoammeter (model 6487, Keithley Instruments, Cleveland). The process was ended by adding a mixture of 1 M HCOOH and 1 M KNO_3 at a current value of 90 nA, after which the membrane was immersed in Milli-Q water to remove residual salts.

Modification of the PET channel with SCCs

Precursor **2** (3 mg) and precursor **3** (12.5 mg) were dissolved in 5 mL dimethyl sulfoxide in a vial and the resulting solution was transferred into the chamber of a conductivity cell containing a PET channel membrane after which the entire apparatus was placed in an oven and heated at 60°C for 48 h. The SCCs-modified PET channel membrane was then removed, washed with ethanol three times and finally immersed in Milli-Q water.

Ion current measurements

The ion currents were measured using a model 6487 picoammeter. These trials involved a device having two chambers similar to a conductivity cell with the chambers separated by the PET channel membrane. The two cells were filled with an electrolyte solution and a transmembrane voltage was applied. The voltage was subsequently varied from − 2 to + 2 V with a 20 s period to generate the *I-V* curves. Each test was repeated three times and the average current values at the different potentials are reported herein.

Dual ion permeation experiments

The SCCs-based hybrid channel membrane was sandwiched between the two chambers of the conductivity cell. One compartment faced the tip of the channel and was filled with 2 mL of a feed solution containing 0.1 M KNO_3 and 0.1 M $Mg(NO_3)_2$, while the other compartment was filled with 2 mL

Milli-Q water as the permeate solution. A constant potential of 2 V was applied to the membrane for 24 h using a model 6487 picoammeter *via* platinum electrodes. The ion concentration in the permeation side was determined using inductively coupled plasma optical emission spectrometry.

Declarations

Acknowledgements

This study was financially supported by the National Natural Science Foundation of China (22061018, 21571019), the Natural Science Foundation for Distinguished Young Scholars of Jiangxi Province (20212ACB213003), and the Academic and Technical Leader Plan of Jiangxi Provincial Main Disciplines (20212BCJ23004).

Author contributions

Y.S. and Y.L. conceived and designed this work. Y.S., R.H.L., and S.Q.C conducted the experiments. Z.C and Y.X performed the computational investigations. H.Q. and X.C.L conducted SEM analysis. Y.S, R.H.L, and Y.L. wrote and revised the manuscript. All authors participated in discussion and reviewed the manuscript before submission.

Competing interests

The authors declare no competing interests.

Additional information

Materials and methods, synthesis and characterizations, experimental procedures, DFT and MD calculation details and supporting figures and tables including NMR spectra, SAXS and pore size distribution data for SCCs **1** and ion measurement details and characterizations for membranes were provided in Supplementary Information.

References

1. Ruan, Z., Osei-Owusu, J., Du, J., Qiu, Z. & Lü, W. Structures and pH-sensing mechanism of the proton-activated chloride channel. *Nature* **588**, 350-354 (2020).
2. Oosterheert, W., Reis, J., Gros, P. & Mattevi, A. An Elegant Four-Helical Fold in NOX and STEAP Enzymes Facilitates Electron Transport across Biomembranes—Similar Vehicle, Different Destination. *Acc. Chem. Res.* **53**, 1969-1980 (2020).
3. Gale, P. A., Davis, J. T. & Quesada, R. Anion transport and supramolecular medicinal chemistry. *Chem. Soc. Rev.* **46**, 2497-2519 (2017).
4. Li, H. et al. Efficient, non-toxic anion transport by synthetic carriers in cells and epithelia. *Nat. Chem.* **8**, 24-32 (2016).

5. Mahendran, K. R. et al. A monodisperse transmembrane α-helical peptide barrel. *Nat. Chem.* **9**, 411-419 (2017).
6. Langton, M. J. Engineering of stimuli-responsive lipid-bilayer membranes using supramolecular systems. *Nat. Rev. Chem.* **5**, 46-61 (2021).
7. Sun, Y. et al. A biomimetic chiral-driven ionic gate constructed by pillar[6]arene-based host–guest systems. *Nat. Commun.* **9**, 2617 (2018).
8. Payandeh, J., Scheuer, T., Zheng, N. & Catterall, W. A. The crystal structure of a voltage-gated sodium channel. *Nature* **475**, 353-358 (2011).
9. Zhang, X. et al. Crystal structure of an orthologue of the NaChBac voltage-gated sodium channel. *Nature* **486**, 130-134 (2012).
10. Pérez-Mitta, G., Toimil-Molares, M. E., Trautmann, C., Marmisollé, W. A. & Azzaroni, O. Molecular Design of solid-state nanopores: fundamental concepts and applications. *Adv. Mater.* **31**, 1901483 (2019).
11. Hou, X., Guo, W. & Jiang, L. Biomimetic smart nanopores and nanochannels. *Chem. Soc. Rev.* **40**, 2385-2401 (2011).
12. Zhu, Z., Wang, D., Tian, Y. & Jiang, L. Ion/molecule transportation in nanopores and nanochannels: from critical principles to diverse functions. *J. Am. Chem. Soc.* **141**, 8658-8669 (2019).
13. Chantiwas, R. et al. Flexible fabrication and applications of polymer nanochannels and nanoslits. *Chem. Soc. Rev.* **40**, 3677-3702 (2011).
14. Hou, Y. & Hou, X. Bioinspired nanofluidic iontronics. *Science* **373**, 628-629 (2021).
15. Powell, M. R., Cleary, L., Davenport, M., Shea, K. J. & Siwy, Z. S. Electric-field-induced wetting and dewetting in single hydrophobic nanopores. *Nat. Nanotechnol.* **6**, 798-802 (2011).
16. Hou, X. Smart Gating multi-scale pore/channel-based membranes. *Adv. Mater.* **28**, 7049-7064 (2016).
17. Gao, P. et al. Regional and functional division of functional elements of solid-state nanochannels for enhanced sensitivity and specificity of biosensing in complex matrices. *Nat. Protoc.* **16**, 4201-4226 (2021).
18. Hou, X., Zhang, H. & Jiang, L. Building bio-Inspired artificial functional nanochannels: from symmetric to asymmetric modification. *Angew. Chem. Int. Ed.* **51**, 5296-5307 (2012).
19. Sun, Y. et al. A light-regulated host–guest-based nanochannel system inspired by channelrhodopsins protein. *Nat. Commun.* **8**, 260 (2017).
20. Guo, W., Tian, Y. & Jiang, L. Asymmetric ion transport through ion-channel-mimetic solid-state nanopores. *Acc. Chem. Res.* **46**, 2834-2846 (2013).
21. Buchsbaum, S. F., Nguyen, G., Howorka, S. & Siwy, Z. S. DNA-modified polymer pores allow pH- and voltage-gated control of channel flux. *J. Am. Chem. Soc.* **136**, 9902-9905 (2014).
22. Zhang, Z. et al. Bioinspired heterogeneous ion pump membranes: unidirectional selective pumping and controllable gating properties stemming from asymmetric ionic group distribution. *J. Am. Chem. Soc.* **140**, 1083-1090 (2018).

23. Lu, J. et al. Efficient metal ion sieving in rectifying subnanochannels enabled by metal–organic frameworks. *Nat. Mater.* **19**, 767-774 (2020).
24. Sato, K., Muraoka, T. & Kinbara, K. Supramolecular transmembrane ion channels formed by multiblock amphiphiles. *Acc. Chem. Res.* **54**, 3700-3709 (2021).
25. Shinde, S. V. & Talukdar, P. A dimeric bis(melamine)-substituted bispidine for efficient transmembrane H^+/Cl^- cotransport. *Angew. Chem. Int. Ed.* **56**, 4238-4242 (2017).
26. Si, W., Xin, P., Li, Z.-T. & Hou, J.-L. Tubular unimolecular transmembrane channels: construction strategy and transport activities. *Acc. Chem. Res.* **48**, 1612-1619 (2015).
27. Qiao, D. et al. Synthetic macrocycle nanopore for potassium-selective transmembrane transport. *J. Am. Chem. Soc.* **143**, 15975-15983 (2021).
28. Lee, L. M. et al. Anion Transport with pnictogen bonds in direct comparison with chalcogen and halogen bonds. *J. Am. Chem. Soc.* **141**, 810-814 (2019).
29. Benz, S. et al. Anion transport with chalcogen bonds. *J. Am. Chem. Soc.* **138**, 9093-9096 (2016).
30. Vargas Jentzsch, A. et al. Ditopic ion transport systems: anion–π interactions and halogen bonds at work. *Angew. Chem. Int. Ed.* **50**, 11675-11678 (2011).
31. Epsztein, R., DuChanois, R. M., Ritt, C. L., Noy, A. & Elimelech, M. Towards single-species selectivity of membranes with subnanometre pores. *Nat. Nanotechnol.* **15**, 426-436 (2020).
32. Yang, Y. et al. Large-area graphene-nanomesh/carbon-nanotube hybrid membranes for ionic and molecular nanofiltration. *Science* **364**, 1057-1062 (2019).
33. Esfandiar, A. et al. Size effect in ion transport through angstrom-scale slits. *Science* **358**, 511-513 (2017).
34. Sun, Y. et al. Inorganic-organic hybrid membrane based on pillararene-intercalated MXene nanosheets for efficient water purification. *Angew. Chem. Int. Ed.* **61**, e2022004 (2022).
35. Li, X. et al. Fast and selective fluoride ion conduction in sub-1-nanometer metal-organic framework channels. *Nat. Commun.* **10**, 2490 (2019).
36. Gopinadhan, K. et al. Complete steric exclusion of ions and proton transport through confined monolayer water. *Science* **363**, 145-148 (2019).
37. Shen, J., Liu, G., Han, Y. & Jin, W. Artificial channels for confined mass transport at the sub-nanometre scale. *Nat. Rev. Mater.* **6**, 294-312 (2021).
38. Chakrabarty, R., Mukherjee, P. S. & Stang, P. J. Supramolecular coordination: self-assembly of finite two- and three-dimensional ensembles. *Chem. Rev.* **111**, 6810-6918 (2011).
39. Bhattacharyya, S. et al. Self-Assembled Pd12 coordination cage as photoregulated oxidase-like nanozyme. *J. Am. Chem. Soc.* **142**, 18981-18989 (2020).
40. Cook, T. R. & Stang, P. J. Recent Developments in the preparation and chemistry of metallacycles and metallacages via coordination. *Chem. Rev.* **115**, 7001-7045 (2015).
41. Sakai, N. & Matile, S. Metal–organic scaffolds: heavy-metal approaches to synthetic ion channels and pores. *Angew. Chem. Int. Ed.* **47**, 9603-9607 (2008).

42. Shen, Y.-x. et al. Achieving high permeability and enhanced selectivity for Angstrom-scale separations using artificial water channel membranes. *Nat. Commun.* **9**, 2294 (2018).
43. Boccalon, M., Iengo, E. & Tecilla, P. Metal–organic transmembrane nanopores. *J. Am. Chem. Soc.* **134**, 20310-20313 (2012).

Figures

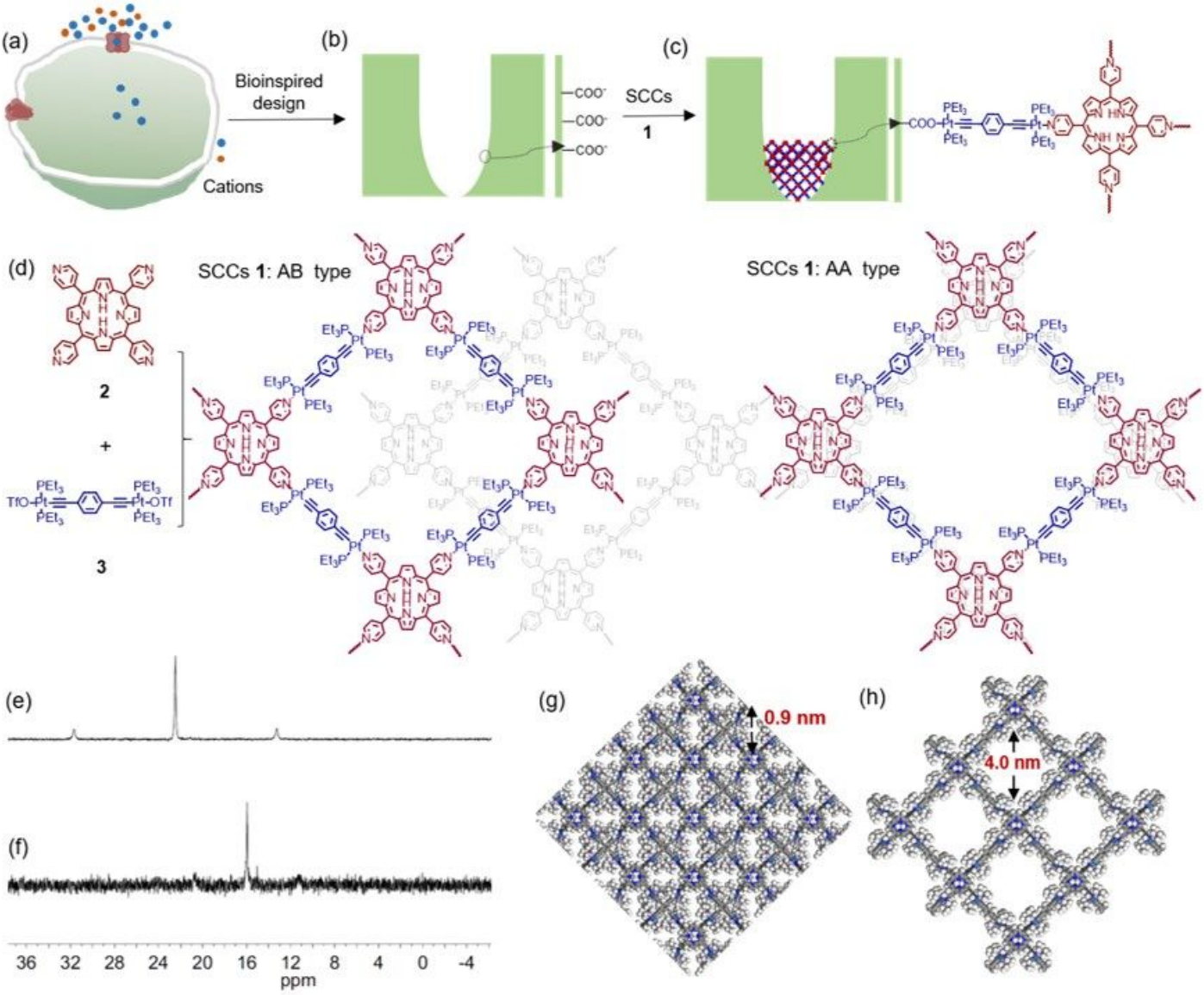

Figure 1

The fabrication of SCCs-based channels. Diagrams of (a) a biological ion channel in an organism, (b) a bare channel, (c) a channel based on SCCs **1** and (d) the synthesis of SCCs **1**. The ^{31}P NMR spectra of (e) ligand **3** and (f) SCCs **1** and (g), (h) structural models of SCCs **1** generated using the Materials Studio software.

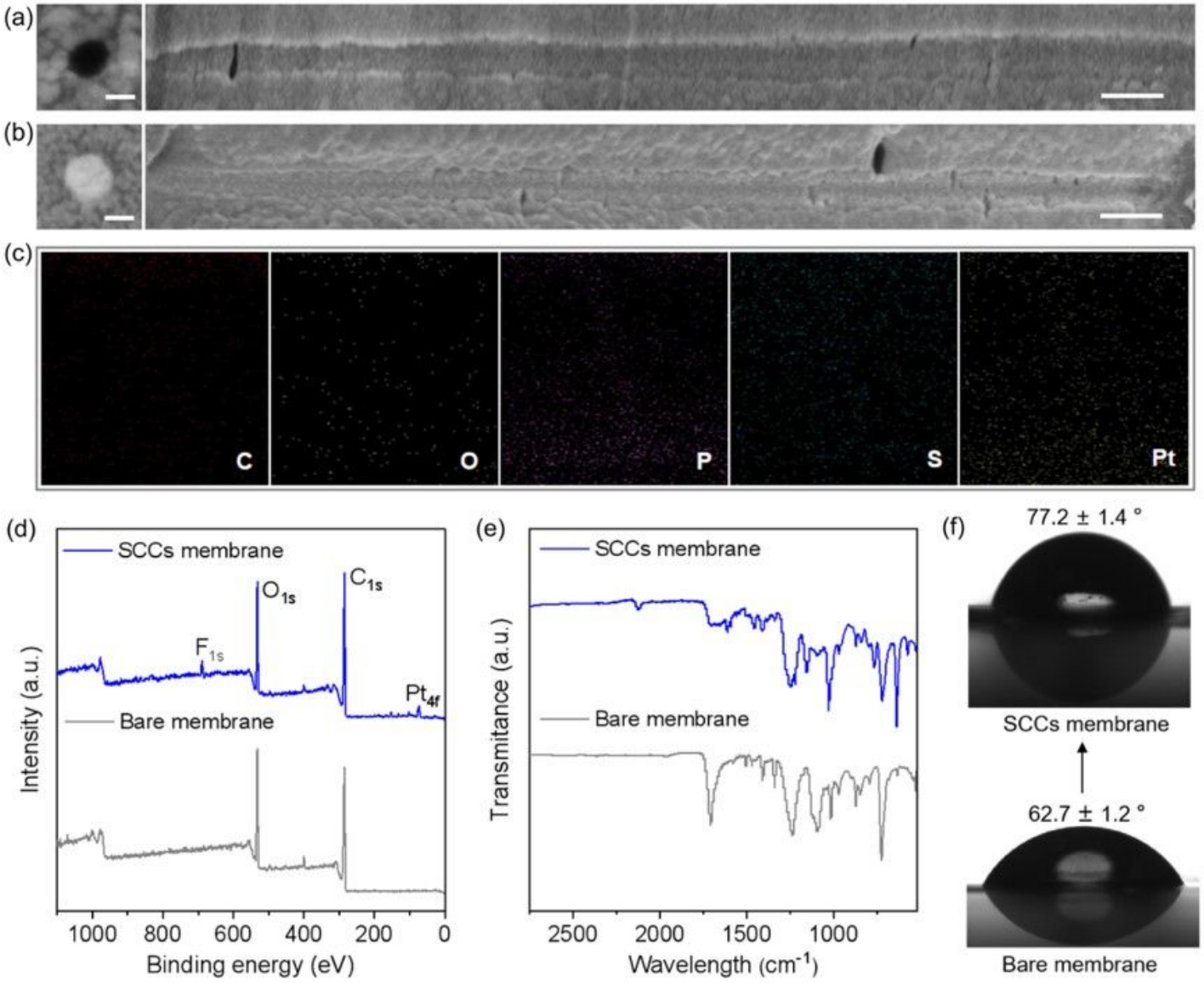

Figure 2

Characterization of the PET membrane before and after applying the SCCs. SEM images of the tip and cross-section of the membrane (a) before and (b) after applying the SCCs, the scales of the tip and cross-section are 50nm and 800nm, respectively. (c) EDS mapping of the treated membrane for C, O, P, S and Pt. (d), (e) and, (f) XPS, FT-IR spectra, and the contact angle on the membrane before and after modification, respectively.

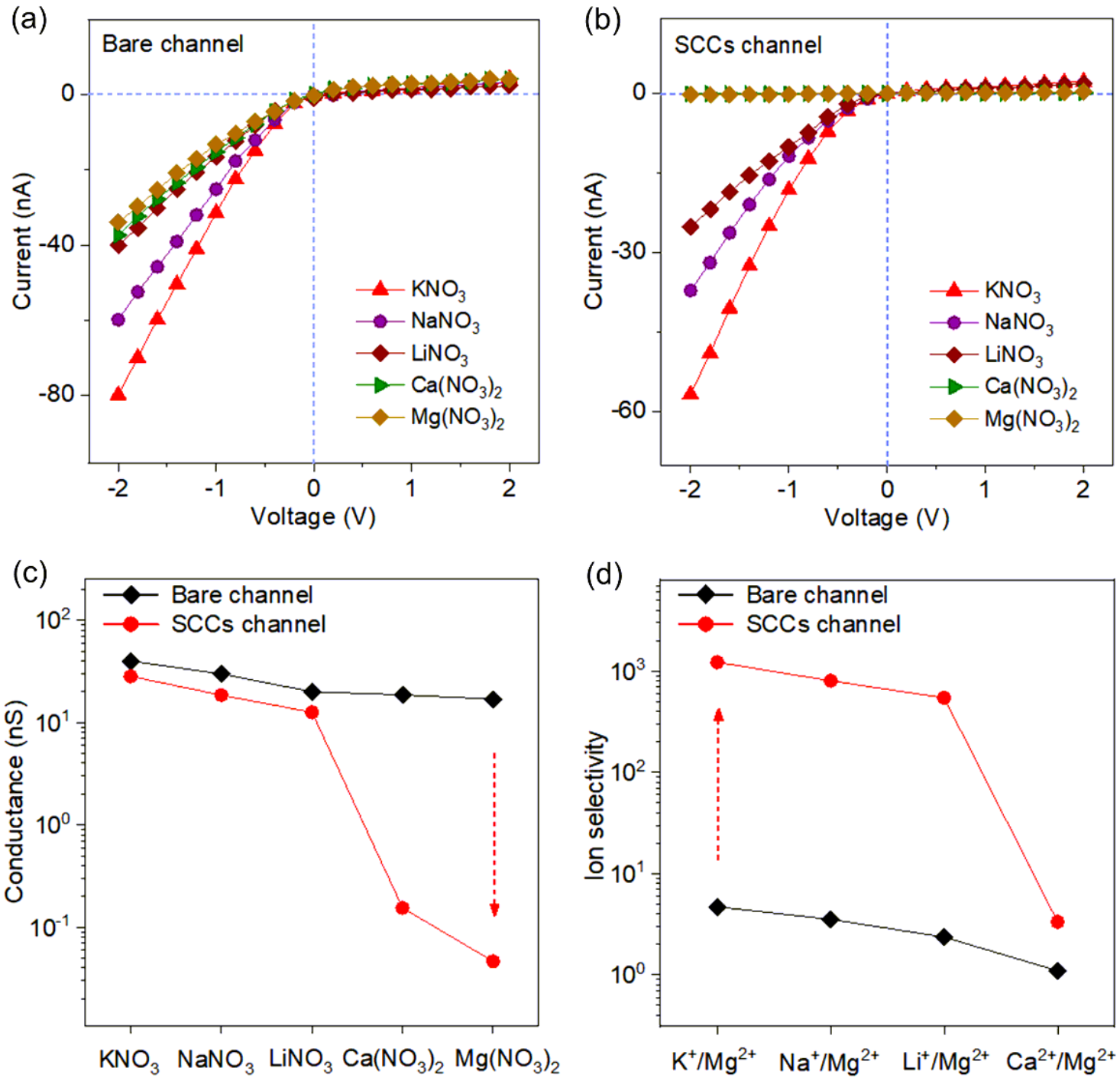

Figure 3

Selective cation transport in the SCCs-based channel. (a), (b) *I-V* curves obtained from a bare channel and an SCCs-based channel monitored in various electrolyte solutions (0.1 M, pH 7), (c) ion conductance values for a bare channel and an SCCs-based channel at -2 V, and (d) ion selectivity values for a bare channel and an SCCs-based channel at -2 V.

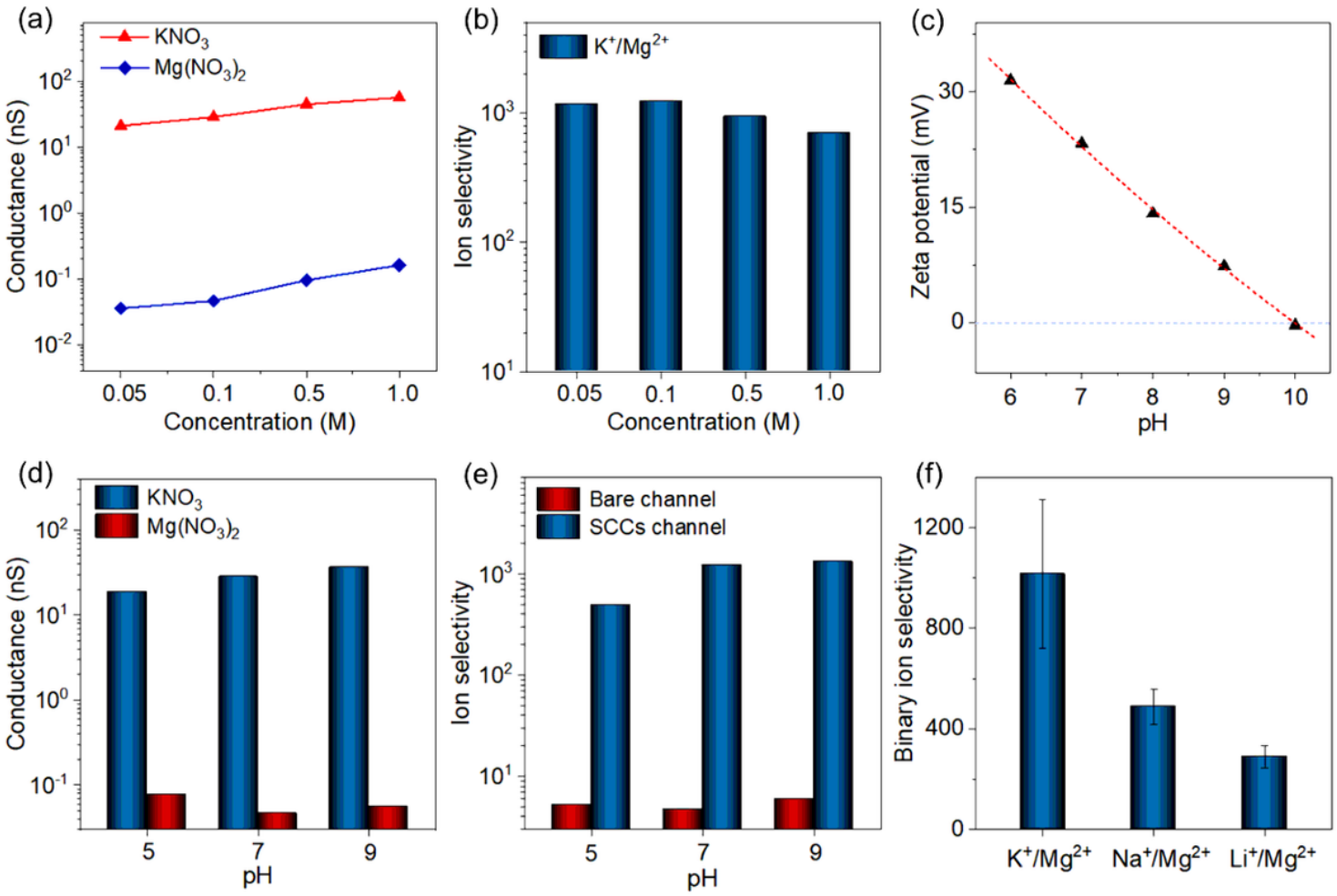

Figure 4

Concentration and pH dependent of ionic transport behavior, and binary ion selectivity of the SCCs channel. (a) KNO_3 and $Mg(NO_3)_2$ conductance of the SCCs channel at various concentrations. (b) Ion selectivity of the SCCs channel at various concentrations. (c) Zeta potential of SCCs toward pH. (d) Influence of pH on KNO_3 and $Mg(NO_3)_2$ conductance in the SCCs channel at −2 V. (e) Influence of pH on K^+/Mg^{2+} selectivity of bare channel and SCCs channel at −2 V. (f) Binary selectivities of the SCCs channel.

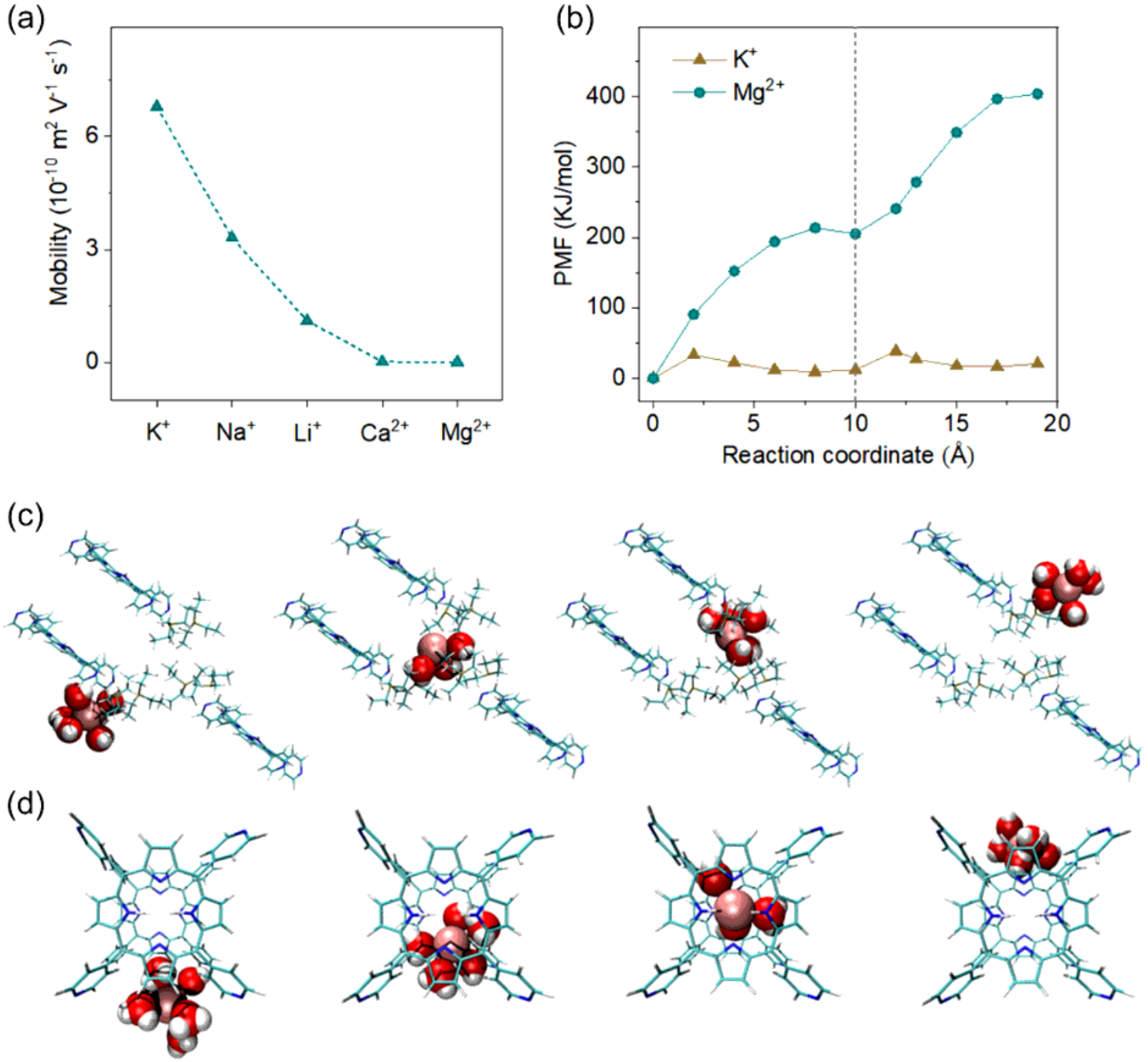

Figure 5

Ion sieving mechanism in the SCCs-based channel. (a) Cation mobilities calculated using MD simulations, (b) PMF values for metal ions migrating along the channel. Diagrams showing the migrations of metal ions along (c) the center and (d) the edge of the channel.

Supplementary Files

This is a list of supplementary files associated with this preprint. Click to download.

- SupplementaryInformation.docx